Front. Phys.
DOI 10.1007/s11467-013-0318-8

REVIEW ARTICLE

Gold nanocages as multifunctional materials for nanomedicine

Xiaohu Xia[1,2], **Younan Xia**[1,2,†]

[1] *The Wallace H. Coulter Department of Biomedical Engineering, Georgia Institute of Technology and Emory University Medical School, Atlanta, GA 30332, USA*

[2] *School of Chemistry and Biochemistry, School of Chemical and Biomolecular Engineering, Georgia Institute of Technology, Atlanta, GA 30332, USA*

E-mail: [†]*younan.xia@bme.gatech.edu*

Received March 2, 2013; accepted March 12, 2013

Featured by tunable localized surface plasmon resonance peaks in the near-infrared region and hollow interiors, Au nanocages represent a novel class of multifunctional nanomaterials that have gained considerable attention in recent years. This short review summarizes our recent work on the capabilities of Au nanocages in nanomedicine. We start with a brief description of the synthesis of Au nanocages and highlight our recent protocols for the scaled-up production of Au nanocages. We then use a number of examples to illustrate how Au nanocages can contribute to nanomedicine with respect to both diagnosis and therapy.

Keywords gold nanocage, nanomedicine, diagnosis, therapy

PACS numbers 81.07.Bc, 87.50.ux, 87.50.ct

Contents

1 Introduction

The essence of medicine is to apply science or technology to the diagnosis and treatment of diseases in human beings. Owing to the great advances in both nanoscience and nanotechnology over the past few decades, nanomedicine, known as the medical applications of nanomaterials (i.e., nanoscale materials with sizes of 1–100 nm), has emerged as a novel and important subfield of modern medicine [1–5]. There are a number of benefits in using nanomaterials in medicine. For example, smaller materials are less invasive, well-suited in functionalization with biomolecules, and much easier to be eliminated from the body.

Because of many merits such as a high degree of size and shape control, easily functionalized surface, and low cytotoxicity, Au nanostructures have proven to be a versatile and multifaceted platform for a variety of applications in nanomedicine [6–9]. Most of these applications are based on an optical phenomenon known as localized surface plasmon resonance (LSPR) [10]. When a Au nanostructure is illuminated with electromagnetic wave of an appropriate wavelength, its conduction electrons will be driven by the electric field to collectively oscillate relative to the lattice of positive nuclei, creating intense extinction peaks (extinction = absorption + scattering) at resonant wavelengths [11, 12]. For *in vivo* medical applications, the LSPR peaks of Au nanostructures should be tuned to the near-infrared (NIR) region ranging from 700 to 900 nm. In this so-called "transparent window", light can penetrate deeply into soft tissues due to the great reduction in absorption from hemoglobin (blood) and water and in scattering from the tissue [13, 14]. Conventional Au colloids with solid structure, spherical shape, and sizes of 5–100 nm typically display LSPR

peaks in the visible region (*ca.* 500–600 nm) [15]. Only those Au nanostructures having non-spherical morphologies (e.g., rod, plate, multipod, and star) or hollow structure (e.g., shell, box, cage, and frame) can have LSPR peaks in the NIR region [10].

Gold nanocages represent a novel class of nanostructures that were invented by our group in 2002 [16, 17]. They can be facilely prepared using a synthetic route involving the galvanic replacement between Ag nanocubes and an aqueous $HAuCl_4$ solution [18]. In addition to the tunable LSPR peaks in a broad range of 600–1200 nm, Au nanocages have many unique features that make them attractive for nanomedicine: i) they can be produced in large quantities (up to ∼0.7 g per batch of synthesis) and high quality (standard deviation of size <15%); ii) their porous walls and hollow interiors can be utilized for the loading and release of drugs; iii) their sizes can be readily controlled from 20 to 500 nm, allowing for optimizing biodistribution and particle permeation through tissues; iv) their LSPR peaks can be dominated by either absorption or scattering to adapt to different imaging modalities; v) they are single crystals with good mechanical flexibility and stability, making them easy to survive complex *in vivo* environments; vi) they have atomically flat surfaces that are suitable for quantitative functionalization and labeling with biomolecules and ligands. In this short review, we discuss some of our recent studies on Au nanocages (AuNCs) with a focus on their capabilities in nanomedicine.

2 Synthesis of Au nanocages

Gold nanocages can be easily prepared through the galvanic replacement reaction between Ag nanocubes and $HAuCl_4$ in an aqueous solution, owing to a favorable difference in electrochemical potential between Ag/Ag^+ (0.80 V) and $AuCl_4^-/Au$ (1.00 V):

$$3Ag_{(s)} + AuCl_{4\,(aq)}^- \rightarrow Au_{(s)} + 3Ag_{(aq)}^+ + 4Cl_{(aq)}^- \quad (1)$$

The galvanic replacement reaction can be conducted in a fashion like titration, with $HAuCl_4$ solution being controllably added into a boiling suspension of Ag nanocubes with a syringe pump. Upon reacting with $HAuCl_4$, the Ag nanocubes would undergo a series of morphological and structural changes as shown in Fig. 1(a) due to the interplay of alloying and dealloying [19]. Detailed discussions can be found in our previous publications [20].

For *in vivo* studies, one of the challenges is to produce Au nanocages in large quantities while maintaining good uniformity in terms of both size and shape. Apparently, the key is to scale up the synthesis of Ag nanocubes without compromising the quality. Since our first publication in 2002 [17], the polyol method has been proven to be a robust route to the synthesis of Ag nanocubes. The synthesis was typically conducted by reducing silver nitrate ($AgNO_3$, a precursor to Ag atoms) with ethylene glycol (EG, a solvent and a source of reductant owing to the formation of glycolaldehyde [21]) in the presence of both poly(vinyl pyrrolidone) (PVP, a stabilizer and capping agent for the Ag(100) surface [22]) and chloride ions (Cl^-, an etchant associated with the O_2 from air for selectively removal of twinned Ag seeds [23]). In recent years, we have further refined the chloride-mediated polyol synthesis by i) adding a trace amount of S^{2-} or HS^- into the reaction system, where Ag_2S

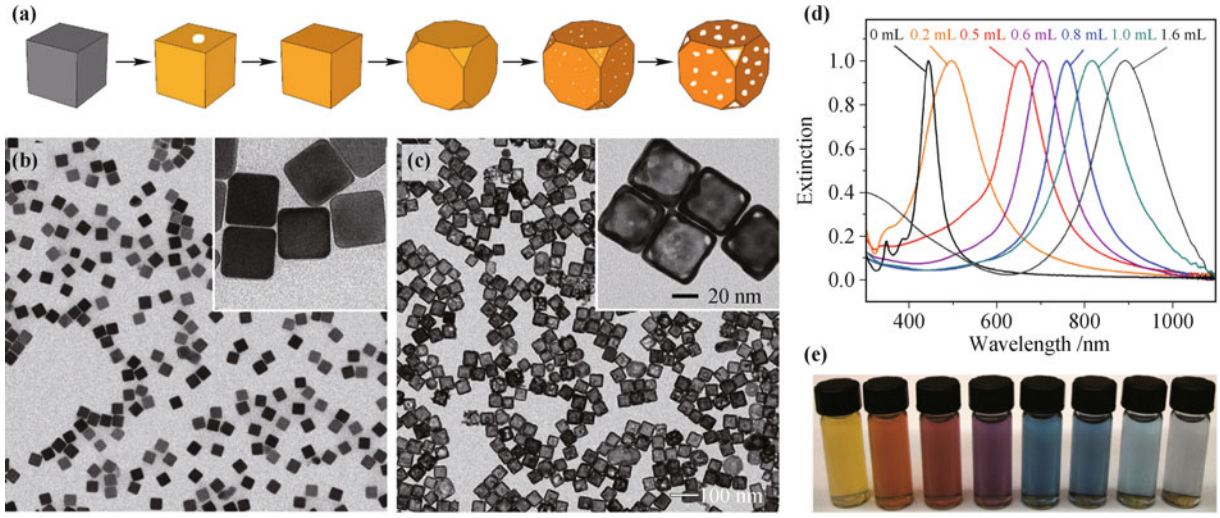

Fig. 1 Synthesis and characterization of Au nanocages. **(a)** Schematic illustration of the structural changes involved in the galvanic replacement reaction between an Ag nanocube and aqueous $HAuCl_4$. **(b)** and **(c)** Representative TEM images of Ag nanocubes and Au nanocages, respectively. **(d)** UV-vis spectra of samples prepared with the addition of different amounts of aqueous $HAuCl_4$ solution. **(e)** Photographs of vials containing the same samples as shown in (d). (d) and (e) are reproduced from Ref. [19], Copyright © 2007 Nature Publishing Group.

nanocrystallites formed at the very beginning could serve as nuclei to help generate single-crystal Ag seeds [24, 25]; and ii) replacing $AgNO_3$ with silver trifluoroacetate (CF_3COOAg), which allowed us to exclude the involvement of NO_2 and other gaseous species derived from the decomposition of nitrate group that may cause unwanted effects on the nucleation and growth processes [26]. With this new protocol, we can routinely produce uniform Ag nanocubes with edge lengths controlled in the range of 30–70 nm, on the scale of 1 gram per batch of synthesis, and within approximately one hour [Fig. 1(b)].

The entire batch of Ag nanocubes (1 gram) could then be placed in a 1000 mL flask and transformed into Au nanocages (∼0.7 gram) by titration with $HAuCl_4$ solution at 80–100°C [Fig. 1(c)]. The extent of replacement could be readily and tightly monitored by taking UV-vis-NIR spectra of aliquots sampled at different volumes of $HAuCl_4$ solution. Figure 1(d) shows the typical shift in LSPR peak position throughout the visible and into the NIR region as the volume of $HAuCl_4$ solution was increased. Accordingly, the samples displayed distinct color changes from yellow to red, purple, and blue [Fig. 1(e)].

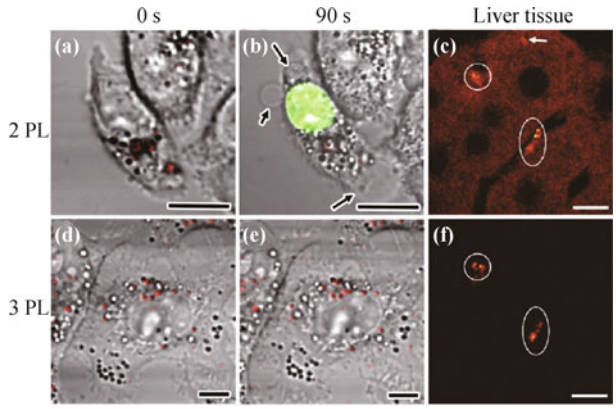

Fig. 2 Comparison of two- and three-photon luminescence (2PL and 3PL) imaging of Au nanocages in (a, b, d, e) KB cells and (e, f) liver tissues. **(a)** 2PL image and **(d)** 3PL image of Au nanocages (red) in KB cells before laser scanning. **(b)** 2PL image of the same cell as in (a) after scanning with 760 nm femtosecond laser for 90 s. Laser power after objective is 1.9 mW. After scanning, we observed membrane blebbing (*arrowed*) and compromised membrane integrity as indicated by ethidium bromide labeling (*green*). **(e)** 3PL image of the same cell as in (b) after scanning with 1290 nm femtosecond laser for 90 s. Laser power after objective is 4.0 mW. **(c)** 2PL image of Au nanocages (*white circles*) in liver tissue. **(f)** 3PL image in the same area as in (c), where white arrow indicates strong autofluorescence from tissue. In (c) and (f), laser powers after objective are 7.0 mW. Scale bars in each image are 10 μm. Reproduced from Ref. [29], Copyright © 2010 Wiley-VCH.

3 Applications in imaging and diagnosis

3.1 Two- and three-photon luminescence imaging

Gold nanostructures can be optically excited to emit luminescence through a recombination of excited electrons in the sp- conduction band with holes in the d-band, and this capability can be used for cellular imaging [27]. This luminescence is significantly enhanced when the LSPR peak of Au nanostructures, such as Au nanocages, matches with the wavelength of the photons used to excite the electrons (typically a NIR laser) [28]. Two-photon luminescence (2 PL) imaging provides a simple and effective means to examine and quantify the cellular uptakes of Au nanocages. However, the heat generated from Au nanocages, owing to the overlap between the LSPR peak of Au nanocages and excitation laser in 2 PL, may cause adverse effects on the biological sample [29]. In comparison, the absorbed photons are more effectively used for the generation of luminescence rather than heat in the case of three-photon luminescence (3 PL) [29]. Figure 2 compares the efficiency and photothermal toxicity of 2 PL and 3 PL for imaging Au nanocages in living cells and tissues. Two KB cells with similar density of Au nanocages were illuminated by a 760 nm laser at 1.9 mW for 2 PL imaging and a 1290 nm laser at 4.0 mW for 3 PL imaging. As shown in Fig. 2(a) and (d), Au nanocages in cells could be visualized by both 2 PL and 3 PL with a similar level of intensity. After 90 seconds scanning with 760 nm laser, membrane blebbling occurred as indicated by ethidium bromide staining (shown in green), together with reduced luminescence intensity from Au nanocages [Fig. 2(b)]. In contrast, neither damages to the plasma membrane nor reduction of luminescence intensity was observed during 90 second 3 PL imaging [Fig. 2(e)]. Another advantage of 3 PL imaging is the complete suppression of autofluorescence from the tissue at 1290 nm excitation, making the 3 PL signal from Au nanocages much easier to be resolved. Figure 2(c) and (f) compares the 2 PL and 3 PL micrographs taken from the same liver tissue slice containing Au nanocages. Clearly, 2 PL imaging caused a much stronger background than 3 PL imaging, primarily due to autofluorescence from the tissue.

3.2 Photoacoustic tomography

Photoacoustic tomography (PAT) is a powerful hybrid biomedical imaging modality that offers both strong optical absorption contrast and high ultrasonic resolution [30–32]. When tissue is irradiated with a pulsed laser source, the resulting heat creates an acoustic signal that can be detected and converted into an image by a scanning transducer. Significantly, the signal can be enhanced by the use of contrast agents that strongly absorb light, such as Au nanostructures [32]. We have

demonstrated the use of Au nanocages as intravascular contrast agents for PAT imaging of cerebral cortex in rat model and sentinel lymph nodes [33]. In a recent study, we demonstrated that the use of [Nle^4, D-Phe^7]-α-melanocyte stimulating hormone ([Nle^4, D-Phe^7]-α-MSH, a melanoma specific peptide) conjugated Au nanocages ([Nle^4, D-Phe^7]-α-MSH-Au nanocages, Fig. 3(a)) as a novel contrast agent for *in vivo* molecular PAT imaging of melanomas with both exquisite sensitivity and high specificity [34]. Figure 3(b) shows an experimental setup of the PAT system, where 10 MHz macroscopic and 50 MHz microscopic dark-field PAT systems were used to image the melanoma and its surrounding microvasculatures, respectively. Figure 3(c) shows a photograph of subcutaneous melanoma in a mouse. After injecting the [Nle^4, D-Phe^7]-α-MSH-Au nanocages into the mouse *via* a tail vein, a series of PAT images were taken from the tumor area up to 6 h post-injection [Fig. 3(d)–(f)]. The melanoma shows significant difference in PA signal enhancement for the [Nle^4, D-Phe^7]-α-MSH-Au nanocages. The average PA signal (golden color) within the melanoma at 6 h post-injection increased by up to 36%. It is worth pointing out that the [Nle^4, D-Phe^7]-α-MSH-Au nanocages enhanced contrast ~300% more than poly(ethylene glycol) (PEG)-Au nanocages (the control), as confirmed by the inductively-coupled plasma mass spectrometry (ICP-MS) data. This observation indicates that Au nanocages can be effectively delivered to a tumor target by modifying their surface with a ligand that specifically binds to a biomarker overexpressed on the tumor surface.

4 Applications in therapy

4.1 Photothermal cancer treatment

Gold nanostructures with LSPR peak in the NIR region are particularly attractive for cancer treatment based on the photothermal effect [35–39]. In the transparent window from 700-900 nm, the incident light can penetrate deeply into soft tissues, ensuring high efficacy for cancer

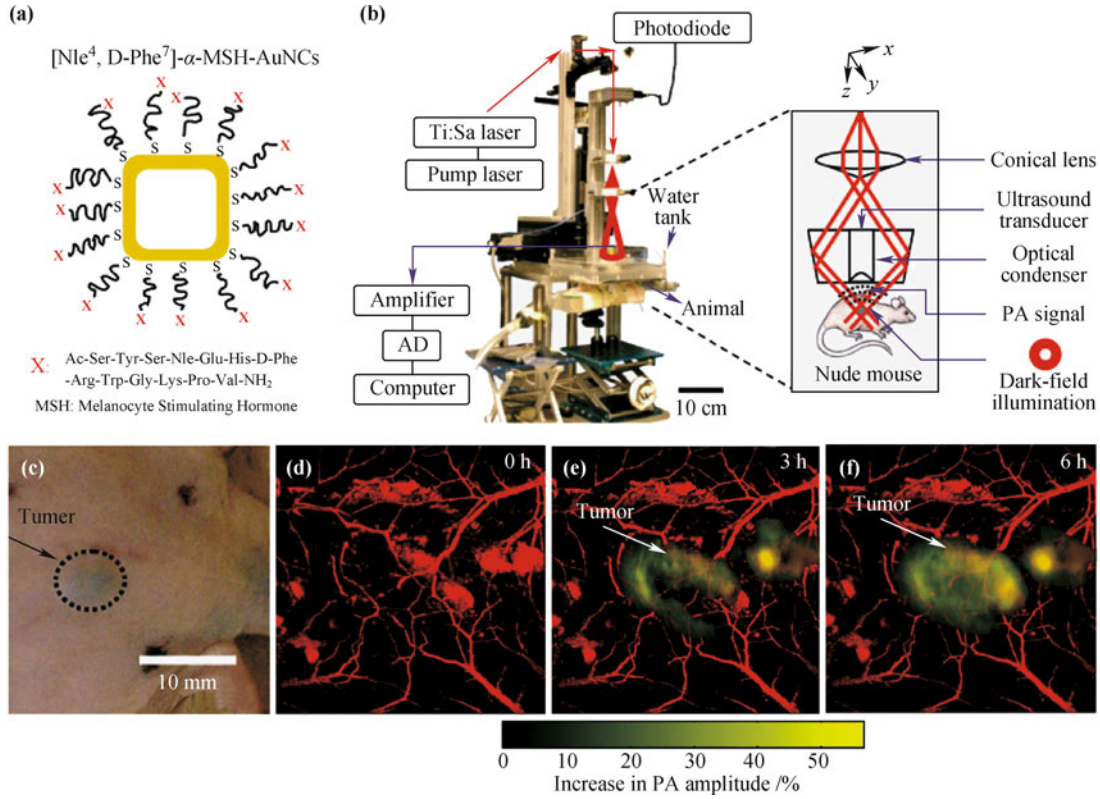

Fig. 3 *In vivo* molecular photoacoustic tomography (PAT) of melanomas using [Nle^4, D-Phe^7]-α-MSH conjugated Au nanocages as contrast agents. **(a)** Schematic drawing of a [Nle^4, D-Phe^7]-α-MSH-Au nanocage. **(b)** Photograph of the PA macroscope. The schematic in the dashed box shows a dark-field, confocal configuration. **(c)** Photograph of nude mice transplanted with B16 melanomas before injection of [Nle^4, D-Phe^7]-α-MSH-Au nanocages. **(d)–(f)** Time-course PA images of the B16 melanomas after intravenous injection with 100 μL of 10 nM of [Nle^4, D-Phe^7]-α-MSH-Au nanocages through the tail vein. The background vasculature images were acquired using the PA microscope at 570 nm (ultrasonic frequency = 50 MHz), and the melanoma images were acquired using the PA macroscope at 778 nm (ultrasonic frequency = 10 MHz). In (d)–(f), red and yellow schemes are for the blood vessels and the increase in PA amplitude, respectively. Reproduced from Ref. [34], Copyright © 2010 American Chemical Society.

treatment with minimum side effects [13]. The key component of this approach is a photothermal transducer capable of absorbing NIR light with a large cross section and then converting the light into heat with high efficiency. Gold nanocages with tunable LSPR peaks in the NIR region are particularly suitable for the use as photothermal transducers, whose NIR absorption cross section can be five orders of magnitude greater than the conventional organic dyes such as indocyanine green [40]. We initially demonstrated the ability of anti-EGFR-conjugated Au nanocages to destroy SK-BR-3 breast cancer cells *in vitro* with the photothermal effect of Au nanocages [39]. More recently, we have investigated the *in vivo* photothermal efficacy of Au nanocages using a bilateral tumor model (Fig. 4) [41]. Experimentally, tumor-bearing mice were intravenously injected with either 100 μL of saline (control) or 100 μL of PEGylated Au nanocages (passive targeting). After 72 h post-injection, the tumor on the right flank of each mouse was subjected to photothermal treatment by exposure to a continuous-wave diode laser at 808 nm at a power density of 0.7 W/cm^2 for 10 min. As monitored by an infrared camera, the tumor containing Au nanocages was rapidly heated to 50 °C within 1 min and then to a plateau temperature at 55°C after 2 min while essentially no change was observed for the control. To evaluate the treatment response, ^{18}F-fluorodeoxyglucose positron emission tomography (^{18}F-FDG PET) was used to monitor the changes in metabolic activity before and after photothermal therapy. Before laser irradiation, ^{18}F-FDG uptake showed no significant difference between saline-injected mice [Fig. 4(a)] and Au nanocages-injected mice [Fig. 4(b)]. At 24 h post-laser treatment, ^{18}F-FDG uptake in tumors of Au nanocages-injected mice [Fig. 4(d)] was significantly reduced as compared to that of saline-injected mice [Fig. 4(c)]. In order to minimize the variation of uptake at different time points, we then normalized the PET signal of the laser-treated tumor to that of the untreated tumor [Fig. 4(e)]. The normalized values of ^{18}F-FDG uptake for Au nanocages-injected mice suggested a decrease in metabolic activity by 70%, while showed no change for the saline-injected mice, indicating there is no benefit for laser treatment in the absence of Au nanocages.

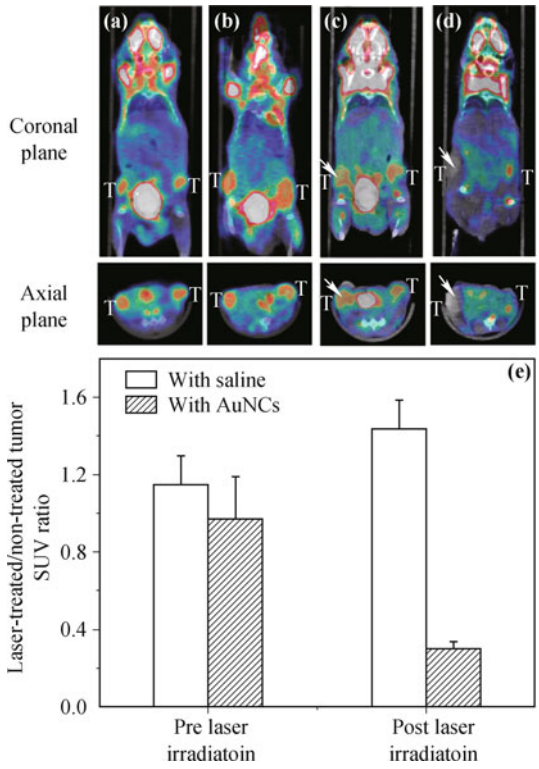

Fig. 4 Gold nanocages for photothermal cancer treatment. ^{18}F-FDG PET/CT co-registered images of mice bearing breast cancer intravenously administrated with either saline or Au nanocages, followed by laser treatment: A saline-injected mouse **(a)** prior to and **(c)** after laser irradiation; An Au nanocages-injected mouse **(b)** prior to and **(d)** after laser irradiation. The white arrows indicated the tumors that were exposed to the diode laser at a power density of 0.7 W/cm^2 for 10 min. **(e)** A plot showing the ratios of laser-treated tumor to non-treated tumor for ^{18}F-FDG standardized uptake values (SUV, P <0.001). Reproduced from Ref. [41],

4.2 Controlled drug release

By taking advantage of their hollow interiors and photothermal effect, Au nanocages have been used as a novel class of drug delivery vehicles. This feature is particularly attractive for nanomedicine because Au nanocages can be monitored with optical imaging techniques while a drug is released at the targeted site. We initially functionalized the surface Au nanocages with thermally responsive polymers to control the release of a drug loaded in the interiors by NIR laser irradiation or high-intensity focused ultrasound (HIFU) [42]. Recently, we demonstrated another interesting controlled drug release system by filling the hollow interiors of Au nanocages with a drug-doped phase-change material (PCM) such as 1-tetradecanol which has a melting point of 38–39 °C [43]. PCMs with a surfactant-like structure, such as those containing both long hydrophobic tails and hydrophilic heads, are preferred to ensure good miscibility with drug molecules. As long as the drug is miscible with the PCM, it can be easily loaded into the Au nanocages *via* the diffusion of PCM-drug mixture. Since the physical state of a PCM can be reversely changed over a narrow temperature range, it can confine the preloaded drug molecules inside the Au nanocages until it is heated to a temperature beyond its melting point, resulting in the release of drug through diffusion [Fig. 5(a)]. As shown in Fig. 5(b), the release can be readily controlled by varying the power of HIFU or the duration of exposure to HIFU.

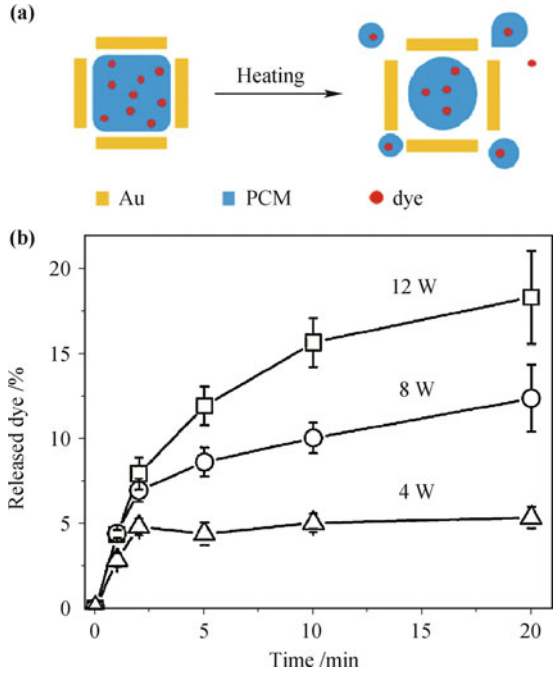

Fig. 5 Gold nanocages as delivery vehicles for controlled drug release. **(a)** Schematic illustration of the loading and then release of a dye from an Au nanocage through the assistance of a phase-change material (PCM). **(b)** Release profiles of the dye exposed to high-intensity focused ultrasound (HIFU) at different applied powers and time points. Reproduced from Ref. [43], Copyright © 2011 American Chemical Society.

5 Conclusions and outlook

Gold nanocages represent a new class of ideal nanomaterials for a variety of applications in nanomedicine due to their unique properties and multifunctional nature. Great progress has been made in this field in recent years: they can be used as optical tracers or contrast agents for various imaging and diagnostic modalities; they can kill cancer cells through the photothermal effect; they can be used to load and release drugs in a controlled manner. With the experiences during the past decade, we now have a better understanding on how to optimize the properties of Au nanocages for a specific application through size/shape-controlled synthesis, surface modification and conjugation of targeting ligands. We believe that the unique features of Au nanocages will likely make them a platform nanomaterial for a range of theranostic applications in nanomedicne. The greatest challenge now is to enhance our understanding of the behaviors and fate of Au nanocages in complex *in vivo* environments, and further extend their capability to clinical use.

Acknowledgements This work was supported in part by an NIH Director's Pioneer Award (DP1 OD00798) and a grant from NCI (R01 CA13852701), and startup funds from Georgia Institute of Technology.

References

1. K. Riehemann, S. W. Schneider, T. A. Luger, B. Godin, M. Ferrari, and H. Fuchs, Angew. Chem. Int. Ed., 2009, 48: 872
2. S. M. Moghimi, A. C. Hunter, and J. C. Murray, FASEB J., 2005, 19(3): 311
3. N. L. Rosi and C. A. Mirkin, Chem. Rev., 2005, 105(4): 1547
4. E. Boisselier and D. Astruc, Chem. Soc. Rev., 2009, 38(6): 1759
5. O. C. Farokhzad and R. Langer, Adv. Drug Deliv. Rev., 2006, 58(14): 1456
6. S. E. Skrabalak, J. Chen, L. Au, X. Lu, X. Li, and Y. Xia, Adv. Mater., 2007, 19(20): 3177
7. S. Lal, S. E. Clare, and N. J. Halas, Acc. Chem. Res., 2008, 41(12): 1842
8. P. K. Jain, X. Huang, I. H. El-Sayed, and M. A. El-Sayed, Acc. Chem. Res., 2008, 41(12): 1578
9. C. J. Murphy, A. M. Gole, J. W. Stone, P. N. Sisco, A. M. Alkilany, E. C. Goldsmith, and S. C. Baxter, Acc. Chem. Res., 2008, 41(12): 1721
10. C. M. Cobley, J. Chen, E. C. Cho, L. V. Wang, and Y. Xia, Chem. Soc. Rev., 2011, 40(1): 44
11. K. Kelly, E. Coronado, L. Zhao, and G. C. Schatz, J. Phys. Chem. B, 2003, 107: 668
12. B. J. Wiley, S. H. Im, Z. Y. Li, J. McLellan, A. R. Siekkinen, and Y. Xia, J. Phys. Chem. B, 2006, 110(32): 15666
13. R. Weissleder, Nat. Biotechnol., 2001, 19(4): 316
14. M. Hu, J. Chen, Z. Y. Li, L. Au, G. V. Hartland, X. Li, M. Marquez, and Y. Xia, Chem. Soc. Rev., 2006, 35(11): 1084
15. J. Rodríguez-Fernández, J. Pérez-Juste, F. J. García de Abajo, and L. M. Liz-Marzán, Langmuir, 2006, 22(16): 7007
16. Y. Sun, B. T. Mayers, and Y. Xia, Nano Lett., 2002, 2: 481
17. Y. Sun and Y. Xia, Science, 2002, 298(5601): 2176
18. Y. Sun and Y. Xia, J. Am. Chem. Soc., 2004, 126(12): 3892
19. S. E. Skrabalak, L. Au, X. Li, and Y. Xia, Nat. Protoc., 2007, 2(9): 2182
20. S. E. Skrabalak, J. Chen, Y. Sun, X. Lu, L. Au, C. M. Cobley, and Y. Xia, Acc. Chem. Res., 2008, 41(12): 1587
21. S. E. Skrabalak, B. J. Wiley, M. Kim, E. V. Formo, and Y. Xia, Nano Lett., 2008, 8(7): 2077
22. X. Xia, J. Zeng, L. K. Oetjen, Q. Li, and Y. Xia, J. Am. Chem. Soc., 2012, 134(3): 1793
23. B. Wiley, T. Herricks, Y. Sun, and Y. Xia, Nano Lett., 2004, 4: 1733
24. A. R. Siekkinen, J. M. McLellan, J. Chen, and Y. Xia, Chem. Phys. Lett., 2006, 432(4–6): 491
25. Q. Zhang, C. Cobley, L. Au, M. McKiernan, A. Schwartz, L. P. Wen, J. Chen, and Y. Xia, ACS Appl. Mater. Interfaces, 2009, 1(9): 2044
26. Q. Zhang, W. Li, L. P. Wen, J. Chen, and Y. Xia, Chem. Eur. J., 2010, 16(33): 10234
27. A. Mooradian, Phys. Rev. Lett., 1969, 22: 185

28. L. Au, Q. Zhang, C. M. Cobley, M. Gidding, A. G. Schwartz, J. Chen, and Y. Xia, ACS Nano, 2010, 4(1): 35
29. L. Tong, C. M. Cobley, J. Chen, Y. Xia, and J.X. Cheng, Angew. Chem. Int. Ed., 2010, 49: 3485
30. X. Yang, E. W. Stein, S. Ashkenazi, and L. V. Wang, Wiley Interdiscip. Rev. Nanomed. Nanobiotechnol., 2009, 1(4): 360
31. K. H. Song, C. Kim, C. M. Cobley, Y. Xia, and L. V. Wang, Nano Lett., 2009, 9(1): 183
32. C. Kim, C. Favazza, and L. V. Wang, Chem. Rev., 2010, 110(5): 2756
33. X. Yang, S. E. Skrabalak, Z. Y. Li, Y. Xia, and L. V. Wang, Nano Lett., 2007, 7(12): 3798
34. C. Kim, E. C. Cho, J. Chen, K. H. Song, L. Au, C. Favazza, Q. Zhang, C. M. Cobley, F. Gao, Y. Xia, and L. V. Wang, ACS Nano, 2010, 4(8): 4559
35. L. R. Hirsch, R. J. Stafford, J. A. Bankson, S. R. Sershen, B. Rivera, R. E. Price, J. D. Hazle, N. J. Halas, and J. L. West, Proc. Natl. Acad. Sci. USA, 2003, 100(23): 13549
36. X. Huang, P. K. Jain, I. H. El-Sayed, and M. A. El-Sayed, Lasers Med. Sci., 2008, 23(3): 217
37. X. Huang, I. H. El-Sayed, W. Qian, and M. A. El-Sayed, J. Am. Chem. Soc., 2006, 128(6): 2115
38. W. Hasan, C. L. Stender, M. H. Lee, C. L. Nehl, J. Lee, and T. W. Odom, Nano Lett., 2009, 9(4): 1555
39. J. Chen, D. Wang, J. Xi, L. Au, A. Siekkinen, A. Warsen, Z. Y. Li, H. Zhang, Y. Xia, and X. Li, Nano Lett., 2007, 7(5): 1318
40. J. Chen, F. Saeki, B. J. Wiley, H. Cang, M. J. Cobb, Z. Y. Li, L. Au, H. Zhang, M. B. Kimmey, X. Li, and Y. Xia, Nano Lett., 2005, 5(3): 473
41. J. Chen, C. Glaus, R. Laforest, Q. Zhang, M. Yang, M. Gidding, M. J. Welch, and Y. Xia, Small, 2010, 6(7): 811
42. M. S. Yavuz, Y. Cheng, J. Chen, C. M. Cobley, Q. Zhang, M. Rycenga, J. Xie, C. Kim, K. H. Song, A. G. Schwartz, L. V. Wang, and Y. Xia, Nat. Mater., 2009, 8(12): 935
43. G. D. Moon, S. W. Choi, X. Cai, W. Li, E. C. Cho, U. Jeong, L. V. Wang, and Y. Xia, J. Am. Chem. Soc., 2011, 133(13): 4762